TOWARDS FAILURE PATTERN FORMATION IN BRITTLE MATERIALS

M. A. Grinfeld, J. W. McCauley, S. E. Schoenfeld, and T. W. Wright
U.S. Army Research Laboratory
Aberdeen Proving Ground, MD, 21005-5069

ABSTRACT

Several Edge-on Impact (EOI) tests on transparent glasses and polycrystalline ceramics have shown that failure fronts have an extremely rough morphology, including the appearance of spikes. A simple thermodynamic theory has been used to interpret the observed morphological instability of failure fronts. For the case of isotropic phases, the instability criterion can be obtained in explicit form.

1. INTRODUCTION

When a high-speed projectile impacts a brittle material, such as glass or polycrystalline ceramic, severe damage and fragmentation is normally observed before projectile penetrates. Several types of transparent glasses have already been studied using the EOI test (Senf, et al, 1997; Strassburger, 2006). Fused silica and AlON is a material being considered for a variety of transparent armor, sensor window, and radome applications. It is a polycrystalline ceramic that fulfills the requirements of transparency and requisite mechanical properties for transparent armor against armor piercing ammunition. AlON has a cubic, spinel crystal structure (Fd3m) that can be processed to transparency in a polycrystalline microstructure. It differs from glasses which do not have any periodic crystalline order, but it is akin to polycrystalline opaque ceramics, such as aluminum oxide.

AlON was recently investigated by Strassburger, Patel, McCauley, and Templeton (2006) using EOI test in two different optical configurations. In the first, a regular transmitted-light shadowgraph set-up was used to observe wave and damage propagation. In the second, a modified configuration was used, where the specimens were placed between crossed polarizers, and the photoelastic effect was utilized to visualize the stress waves. Pairs of impact tests at approximately equivalent velocities were carried out in transmitted plane light (shadowgraphs) and crossed polarized light.

AlON and fused silica specimens were impacted using solid cylinder steel projectiles with velocities ranging from 270 to 925 m/s.
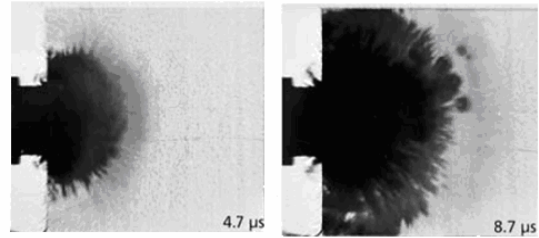
a) shadowgraphs
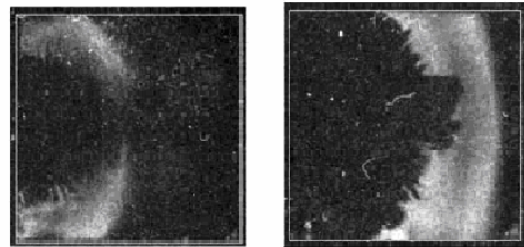
b) cross-polarized light

Figure 1. Selection of two shadowgraphs and corresponding crossed polarizers pictures from impact on AlON at 380 m/s

The nucleation of crack centers was observed ahead of the apparent fracture front, growing from the impacted edge of the specimens. A comparison of the shadowgraphs the photographs (recorded in a reflected light configuration with a coated AlON specimen at the same impact conditions) indicated fracture nucleation in the interior of the ceramic.

Figure 1 shows a selection of two regular shadowgraphs along with the corresponding crossed polarizer photographs for tests with AlON at 380 m/s. The high-speed photographs show rapidly growing darkened to opaque regions, which reflect changes in the optical transmission due to pressure-induced refractive index changes and damage and fractured zones within the specimen. In addition, the nucleation of crack centers ahead of the crack front is clearly visible 8.7 µs after impact. In contrast to the shadowgraphs, where a wave front is not

1. REPORT DATE **01 NOV 2006**	2. REPORT TYPE **N/A**	3. DATES COVERED **-**

4. TITLE AND SUBTITLE **Towards Failure Pattern Formation In Brittle Materials**	5a. CONTRACT NUMBER
	5b. GRANT NUMBER
	5c. PROGRAM ELEMENT NUMBER
6. AUTHOR(S)	5d. PROJECT NUMBER
	5e. TASK NUMBER
	5f. WORK UNIT NUMBER
7. PERFORMING ORGANIZATION NAME(S) AND ADDRESS(ES) **U.S. Army Research Laboratory Aberdeen Proving Ground, MD, 21005-5069**	8. PERFORMING ORGANIZATION REPORT NUMBER
9. SPONSORING/MONITORING AGENCY NAME(S) AND ADDRESS(ES)	10. SPONSOR/MONITOR'S ACRONYM(S)
	11. SPONSOR/MONITOR'S REPORT NUMBER(S)

12. DISTRIBUTION/AVAILABILITY STATEMENT **Approved for public release, distribution unlimited**

13. SUPPLEMENTARY NOTES **See also ADM002075., The original document contains color images.**

14. ABSTRACT

15. SUBJECT TERMS

16. SECURITY CLASSIFICATION OF:			17. LIMITATION OF ABSTRACT **UU**	18. NUMBER OF PAGES **7**	19a. NAME OF RESPONSIBLE PERSON
a. REPORT **unclassified**	b. ABSTRACT **unclassified**	c. THIS PAGE **unclassified**			

discernible, the crossed polarizer's configuration reveals an approximately semicircular stress wave front, which is a little further advanced than the damage front visible in the shadowgraphs at the same time. In the shadowgraph images (Figure 1a) the failure (damage) region clearly exhibits very sharp failure and damage spikes extending out from the front of the main damage region.

2. FORMAL STATEMENT OF THE PROBLEM

In the paper, we suggest a simple thermodynamic theory which explains the appearance of the spikes in the aforementioned experiments with AlON. Two different theoretical and computational approaches seem to be most useful in analyzing different aspects of wave propagation in brittle solids. They describe failure fronts on different spatial length scales. According to the first, less detailed, "macroscopic" approach, the failure front is treated as an infinitely thin mathematical surface separating intact and comminuted spatial domains. According to the second, "microscopic" approach, the failure front has very thin (though still finite) thickness. Within this thin spatial domain, all physical parameters of the substance change continuously but extremely rapidly. Quite often, additional physical processes should be taken into account inside these thin domains, whereas outside these thin domains, the additional physical processes play a relatively minor role. In this respect, the situation with the two-scale description of failure waves is the same as with the classical hydrodynamic and combustion/ detonation shock waves (Landau and Lifshitz., 1987; Courant and Friedrichs, 1948).

Although the spatial domain of intensive fracture in the Edge-on Impact AlON experiments are, in fact, quite thick, we begin our analysis with the simpler macroscopic approach. Within each of the spatial domains, the energy densities e_{int} and e_{dam} per unit mass of the intact and damaged states are given by the following quadratic forms of displacement gradients, respectively:

$$\rho e_{in}(u_{m,n}) = (1/2)c_{\text{int}}^{ijkl} u_{i,j} u_{k,l},$$
$$\rho e_{dam}(u_{m,n}) = (1/2)c_{dam}^{ijkl} u_{i,j} u_{k,l} + q_b,\qquad(2.1)$$

where c_{in}^{ijkl} and c_{dam}^{ijkl} are the elasticity tensors of the two states, and ρ is the original mass density (a subscript after comma is used to denote differentiation with respect to the spatial coordinates x^i). Limiting ourselves with the approximation of linear elasticity, we ignore all effects of mass density change. The positive constant q_b takes into account the energy required to produce various defects (interfaces, vacancies, shear bands, holes, etc.) distributed within unit mass of the bulk of damaged substance. This term is analogous to the constant used in the theory of slow combustion, which takes into account the energy release/consumption due to chemical reactions (Landau and Lifshitz., 1987; Courant and Friedrichs, 1948).. See the papers (Grinfeld, and Wright, 2002, 2004) for a more detailed discussion of the model.

In addition to appropriate initial and external boundary conditions, the master system includes

a) the bulk momentum equation within each of the bulk domains,

$$\rho \frac{\partial^2 u^i}{\partial t^2} = \frac{\partial p^{ji}}{\partial x^j},\qquad(2.2)$$

b) the displacement continuity equation across the failure front,

$$\left[u^i\right]_-^+ n_j = 0,\qquad(2.3)$$

c) and the momentum continuity across the failure front,

$$c\left[\frac{\partial u^i}{\partial t}\right]_-^+ + \left[p^{ji}\right]_-^+ n_j = 0,\qquad(2.4)$$

where $p^{ji} = \partial e(u_{m,n})/\partial u_{i,j}$ is the stress tensor, and n_i is the unit normal to the failure front.

The last equation across the failure front describes the kinetics of failure as follows:

$$c = -K\left[\mu_{.k}^j\right]_-^+ n_j n^k,\qquad(2.5)$$

where c is the velocity of the failure front, and the tensor $\mu_{.k}^j$ is defined as

2

$$\mu_{.k}^{j} = e\delta_k^j - \rho^{-1}p^{ji}\left(\delta_{ik} + u_{i,k}\right). \qquad (2.6)$$

It plays the same role as the scalar Gibbs chemical potential μ of a liquid substance; K is a positive (kinetic) constant or function with dimension [*velocity*] [1]. We assume explicitly that the displacements and traction remain continuous across the interface. This is not the only reasonable option. Another reasonable option, especially when dealing with highly fragmented states, would be the model of a friction-free interface with discontinuous displacements. In this case the last (kinetic) constitutive equation (2.5) should be modified as well (a similar system was analyzed in the context of phase transformations in the monograph (Grinfeld, 1991)).

We limit our study with two-dimensional propagation and consider an initially resting uniform half-plane, $x \geq 0$, experiencing an impact at $x = 0$ by the oblique force P (see Figure 2).
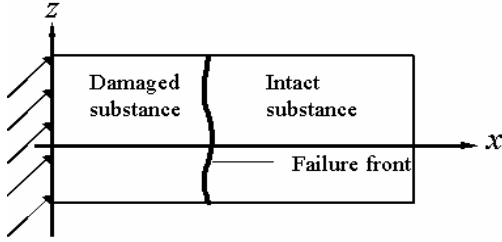
Figure 2. Oblique impact of a brittle substance.

The system (2.2)–(2.6) allows piece-wise linear solutions of the following form:

$$u_+^i(x,z,t) = d_+^i t + a_+^i z \ at \ x \geq ct\,,$$
$$u_-^i(x,z,t) = d_-^i t + a_-^i z \ at \ x \leq ct\,, \qquad (2.7)$$

where $d_\pm^i$, $a_\pm^i$, and c are certain constants. The sign $+(-)$ marks the quantities related to the intact (damaged) state. The constant c gives the speed of the failure front across which the displacement gradients $a_\pm^i$ suffer the finite discontinuities. The solution mentioned above allows the consideration of the quasi-static problem oblique impact (loading) when the

applied force has the components $p_\pm^{xx} = \pi$ and $p_\pm^{zx} = \tau$. The resulting formula is particularly simple and transparent in the quasi-static approximation, i.e., when inertia is neglected in the equations (2.2) and (2.4); then, formula of the velocity of the failure front:

$$\frac{\rho}{K}c = \frac{\pi^2}{2}\left(\frac{1}{\lambda_- + 2\mu_-} - \frac{1}{\lambda_+ + 2\mu_+}\right) +$$
$$\frac{\tau^2}{2}\left(\frac{1}{\mu_-} - \frac{1}{\mu_+}\right) - q_b\,; \qquad (2.8)$$

here $\lambda_\pm$, $\mu_\pm$ are the Lame elastic modules of the intact and comminuted materials that are assumed isotropic. The Poisson ratios are defined as $\nu_\pm = \lambda_\pm / 2(\lambda_\pm + \mu_\pm)$.

3. MORPHOLOGICAL INSTABILITY OF FAILURE FRONT

In order to explore morphological stability of the piece-wise linear solution we present the elastic displacement $u_\pm^i(x,z,t)$ and the speed of the interface $c(z,t)$ in the following form:

$$u_\pm^i(x,z,t) = u_\pm^{\circ i}(x,t) + \widetilde{u}_\pm^i(x,z,t),$$
$$c(x,z,t) = c^\circ + \widetilde{c}(z,t), \qquad (3.1)$$

where $\widetilde{u}_\pm^i(x,z,t)$ and $\widetilde{c}(z,t)$ are small disturbances. The above presentations should be substituted in the bulk equations and in the boundary conditions (1), (2), which should then be linearized with respect to the small disturbances. We then look for the solutions of the linearized system in the following form (k is the in-plane wave-number and η is the rate of growth):

$$\widetilde{u}_\pm^i(x,z,t) = W_\pm^i\left(x - c^\circ t\right)e^{ikz+\eta t},$$
$$\widetilde{c}(z,t) = Se^{ikz+\eta t}, \qquad (3.2)$$

where the functions $W_\pm^i(X)$ should decay exponentially at $X \to \pm\infty$.

The dispersion equation for η is somewhat lengthy and cumbersome without further special

3

assumptions. For the case of isotropic states and two-dimensional geometry it reads as follows:

$$(3.3)$$

$$\frac{K}{k}\eta = \frac{4\mu_-\left(\mu_-^2 - \mu_+^2\right)\left(1 - \nu_-\right)}{\left(3 - 4\nu_-\right)\mu_+^2 + 4\mu_-\mu_+\left(1 - \nu_-\right) + \mu_-^2} -$$

$$8\frac{\tau^2}{\pi^2}\frac{\mu_-\left(\mu_- - \mu_+\right)^2}{\mu_+}\frac{\left(1 - \nu_-\right)^2}{\left(1 - 2\nu_-\right)^2} \times$$

$$\frac{2\mu_+\left(1 - \nu_-\right) + \mu_-}{\left(3 - 4\nu_-\right)\mu_+^2 + 4\mu_-\mu_+\left(1 - \nu_-\right) + \mu_-^2}\ .$$

The last formula becomes relatively compact and instructive in the limit of an incompressible damaged state ($\nu_- = 1/2$) and when in the intact state $\nu_+ = 1/3$. Then, it reads as follows:

$$(3.4)$$

$$\frac{\rho}{8Kk}\eta = \frac{\mu_+\left(\mu_+^2 - \mu_-^2\right)}{5\mu_-^2 + 8\mu_-\mu_+ + 3\mu_+^2} -$$

$$4\frac{\tau^2}{\pi^2}\frac{\mu_+\left(\mu_+ - \mu_-\right)^2}{\mu_-}\frac{4\mu_- + 3\mu_+}{5\mu_-^2 + 8\mu_-\mu_+ + 3\mu_+^2}\ .$$

The wave front is morphologically unstable if the linearized master equation permits solutions of the above form and with the rate η corresponding to exponential growth in time. The last formula (3.4) shows that shear stresses, τ, play a stabilizing role (similar to the case of morphological instabilities of solid-solid phase interfaces, discussed in Grinfeld, 1991). In addition, at $\tau = 0$, the failure front is morphologically unstable in the most interesting case when the shear modulus μ_- of the damaged state is less than the shear modulus μ_+ of the intact state. This instability has a simple physical meaning. It means that penetration of fingers of damaged material into intact material is the fastest way of releasing accumulated elastic energy from the system.

4. INTUITIVE INTERPRETATION OF THE MORPHOLOGICAL INSTABILITY OF FAILURE FRONTS

A plausible interpretation of the stress driven destabilization of failure fronts can be based on the principle of the fastest energy release (or of the entropy production) of irreversible thermodynamics. In the context of fracture, the principle postulates that fracture develops in such a way that the maximum elastic energy should be released (per fixed amount of damaged bonds). Simply stated, the propagation of fingers has a simple physical meaning. It means that penetration of fingers of damaged material into intact material is the fastest way of releasing accumulated elastic energy from the system.
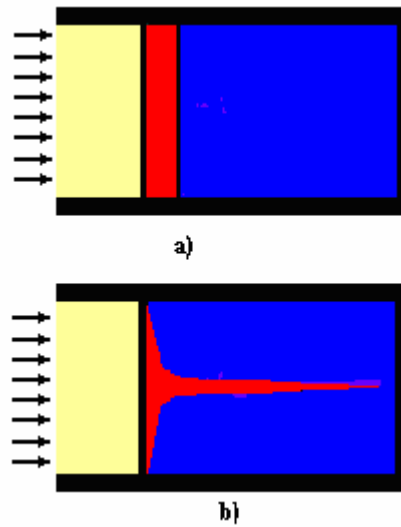
Figure 3. Towards intuitive interpretation of the hackle zone formation.

Figure 3 shows two different morphologies of the advancing front: Figure 3a illustrates an advancing failure front that does not change its morphology and remains flat, and the Figure 3b shows an advancing front in the form of a horizontal finger. It is assumed that the two newly created comminuted areas, shown in red in the figures 3a and 3b, are equal. It should be intuitively clear that the finger-like morphology of the failure front allows much more elastic energy to be released than the morphologically stable front shown on 3a). Indeed, the propagating flat front on 3a) releases the elastic energy only within the small rectangle (between the original and final front positions), whereas the finger-like front allows to release the accumulated elastic energy from everywhere to the right of the original front (including in the material that remains in the intact state). So the

"fingering" of the front allows the accumulated energy to be released in a more efficient way than with the morphologically stable propagation of the flat failure front. This is the potentially possible mechanism of morphological destabilization of the failure front discussed in this paper.

5. CONTINUUM MODEL OF DAMAGE

The model considered above is a certain two-state *discrete* fracture model (Grinfeld and Wright, 2002, 2004). A *continuum* fracture model should include a damage parameter κ that can assume a continuum range of values. Corresponding elastic energy e function is becoming a function of the elastic gradients $u_{i|j}$ and of the damage parameter κ: $e = e(u_{i,j}, \kappa)$. For such a model the bulk equations of equilibrium includes a) the condition of mechanical equilibrium, and b) the equation of "chemical" equilibrium, i.e., of equilibrium with respect of damage proliferation:

a) $\quad \dfrac{\partial}{\partial x^j} \dfrac{\partial e(u_{m,n}, \kappa)}{\partial u_{i,j}} = 0,$ (5.1)

b) $\quad \dfrac{\partial e(u_{m,n}, \kappa)}{\partial \kappa} = 0$. (5.2)

It is more or less typical for the system with damage that full equilibrium with respect to damage proliferation cannot be achieved. In such situations, we have to switch from the equation of chemical equilibrium (5.2) to its quasi-static analogue:

$$\frac{\partial \kappa}{\partial t} = -\eta \frac{\partial e(u_{m,n}, \kappa)}{\partial \kappa} \quad , \quad (5.3)$$

where η is a certain positive kinetic constant.

The important issue here is the choice of an appropriate energy function $e = e(u_{i|j}, \kappa)$. For the purposes of fracture mechanics such a function can be found by combining the approaches of the theories of vacancies in ceramics sintering (Lifshitz, 1963) and of the damage mechanics (Kachanov, 1986).

The quasi-static system presented above was used to numerically explore the behavior of a circular plate with a thin elliptic cavity under action of external pressure for the energy density

$$e(u_{i|j}, \kappa) = \frac{\xi}{2}\left(\kappa - \kappa^\circ\right)^2 +$$
$$\mu\phi(\kappa)\left(\frac{\nu}{1-2\nu}u^i_{\cdot,i}u^j_{\cdot,j} + u_{(i,j)}u^{ij}_{\cdot,\cdot}\right), \quad (5.4)$$

with the *damage function* $\phi(\kappa)$ (Grinfeld and Wright, 2002, 2004)

$$\phi(\kappa) = 1 - \left(1 - c_{\min}\right)\frac{\kappa}{\kappa^*}, \quad (5.5)$$
$$0 \leq \kappa \leq \kappa^*, \quad 0 < c_{\min} \leq 1.$$

Thus, the suggested model depends on 6 constants: μ, ν, ξ, κ°, κ^*, $c_{\min}$. The first two of them are just the shear modulus and Poisson's ratio of the intact substance. The physical meaning of the remaining four constants will be explained elsewhere. For a certain choice of the constants, the evolution of the *relative damage parameter* κ / κ^* is shown in the Figure 4. The depth of gray color reflects the magnitude of the relative damage parameter — white corresponds to a fully damaged material and black to a fully undamaged. Not surprisingly, the largest damage occurs at the tips of the cavity.
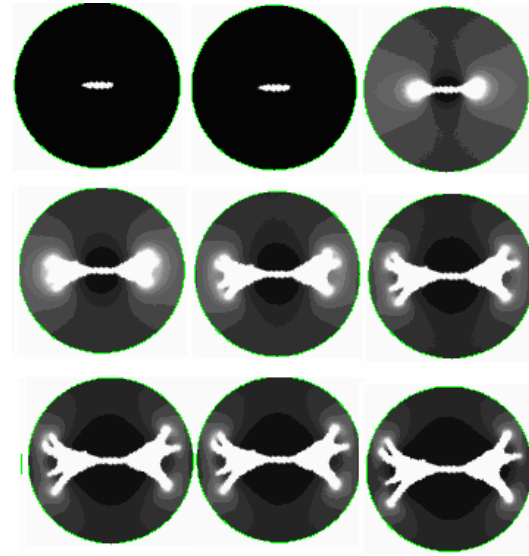

Figure 4. Development of damage in a circular elastic plate with an elliptic cavity.

Figure 5 illustrates developing damages for the case of a brittle ring under the action of different outer and inner pressure. It is very instructive from at least two points of view.

First, this geometry is representative of the important problem of penetration of a rod-like projectile with a circular cross section through a thin brittle isotropic ring.

Second, this example is particularly instructive from the standpoint of morphological instability of failure fronts. The formulated problem is obviously radially symmetric since the intact and damaged states are assumed isotropic, the boundary circles are assumed concentric, and the pressure loading does not violate the radial symmetry. Thus, the problem under consideration possesses a solution describing evolution with radial symmetry. This solution would be easy to model numerically if it were stable with respect to small perturbations of radial symmetry, however, such non-radial small perturbations are always present in any numerical implementation.
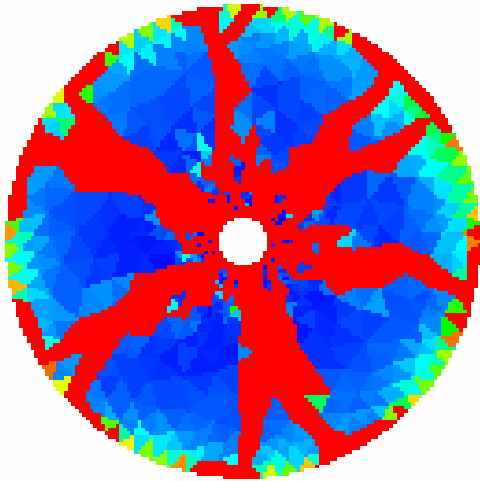
Figure 6. Isotropic brittle ring under unequal outer and inner pressures.

The results of (Grinfeld et al, 2006), briefly presented in the section 3, prompt us to make a conjecture that the radial solution of the system (5.1), (5.2) for the ring under unequal pressures is unstable and cannot be obtained numerically. Figure 6 completely confirms this conjecture. At this early stage of our research, it remains totally unclear what parameters control the number of microcracks in the model. It will be the subject of our future theoretical analysis and numerical experiments.

6. CONCLUSION

A transparent polycrystalline AlON was tested in an Edge-On Impact configuration. Damage propagation was observed in a regular shadowgraph set-up and in a dynamic photoelastic model using crossed polarizers. Photographs recorded in a reflected light configuration with a coated AlON specimen at the same impact conditions confirmed that damage/fracture, and isolated crack nucleation occurred in the interior of the ceramic; the failure (damage) front proceeded through the AlON plate with a spikes-like morphology.

We have presented a simple model for a failure front based on an analogy with slow combustion, and we have presented a formula for the velocity of failure wave generated by oblique impact on a brittle material. We then demonstrated that under rather general assumptions, the flat failure front is morphologically unstable. The last conclusion shows an additional analogy between failure fronts and slow combustion fronts (however, the mechanisms of destabilization are totally different).

Theoretical results, based on the two-state model of damage, have been confirmed by numerical experiments based of the IDZ-models suggested earlier in (Grinfeld and Wright, 2002, 2004)

The morphological instability of failure fronts sheds light on a) the appearance of spikes in the AlON edge-on impact experiments, b) on failure fronts and crack bifurcations as observed in experiments on static indentation of brittle materials, and c) on appearance of radial cracks in dynamic experiments with penetration of projectiles through brittle materials.

This suggests that the investigation into AlON offers insight into damage evolution not only in AlON, but also in other opaque ceramics where only surface damage can be observed with optical methods. Further experimental and theoretical studies are mandatory before making ultimate conclusions.

7. ACKNOWLEDGEMENT

1. Senf, H., Strassburger, E., Rothenhäusler, 1997: A Study of Damage during Impact in Zerodur, *J. PHYS IV*, C3, **7**, 1015-1020.
2. Strassburger, E., 2004: Visualization of Impact Damage in Ceramics Using the Edge-On Impact Technique, *Int. J. of Appl. Cer. Technology*, **1**(3), 235-242.
3. Strassburger1, Patel, P., McCauley, J. W., and Templeton, D. W., 2006: High-Speed Photographic Study of Wave Propagation and Impact Damage in Fused Silica and AlON Using the Edge-on Impact (EOI) Method, Shock Compression in Condenced Matter, AIP Conference Proceeding, **845**.
4. Landau, L.D., and Lifshitz, E.M., 1987: Fluid Mechanics, Pergamon Press, New York.
5. Courant, R., and Friedrichs, K. O., 1948: Supersonic Flow and Shock Waves, Springer-Verlag, New York.
6. Grinfeld, M.A., and Wright, T.W., 2002: Thermodynamics of Solids: Recent Progress with Applications to Brittle Fracture and Nanotechnology, *23th Army Research Conference*, Orlando.
7. Grinfeld, M. A., and Wright, T. W., 2004: Morphology of Fractured Domains in Brittle Fracture, *Metall. Mater. Trans.* A **35**, 2651.
8. Grinfeld, M.A., Thermodynamic Methods in the Theory of Heterogeneous Systems, 1991, Longman,
9. Lifshits, I. M., 1963: Theory of Dynamic-Viscose Yielding of Polycrystalline Solids, *Zh Eksp. Teor. Fiz.*, **44**, 1349-1357.
10. Kachanov, L.M., 1986: Introduction to Continuum Damage Mechanics, Martinus Nijhoff Publishers.
11. Grinfeld, M.A., Schoenfeld, S. E., and Wright, T.W., 2006: Appl. Phys. Lett., **88**, 3396.